PIC SIMULATIONS OF ION DYNAMICS IN ECR ION SOURCES

V. Mironov and J. P.M. Beijers,
Kernfysisch Versneller Instituut, University of Groningen, The Netherlands

Abstract

To better understand the physical processes in ECRIS plasmas, we developed a Particle-in-Cell code that follows the ionization and diffusion dynamics of ions. The basic features of the numerical model are given elsewhere [1]. Electron temperature is a free parameter and we found that its value should be about 1 keV to reproduce the experimentally observed performance of our 14 GHz ECR source. We assume that a pre-sheath is located outside the ECR zone, in which ion acceleration toward the walls occurs. Electric fields inside the ECR zone are assumed to be zero. The ion production is modelled assuming ion confinement by a ponderomotive barrier formed at the boundary of the ECR zone. The barrier height is defined by the RF radiation density at the electron resonance layer and is taken as an adjustable parameter. With these assumptions, we are able to reproduce the main features of ECRIS performance, such as saturation and decrease of highest charge state currents with increasing gas pressure, as well as reaction to an increase of injected RF power. Study of the source response to variations of the source parameters is possible.

INTRODUCTION

Electron Cyclotron Resonance Ion Sources are key components of many accelerator complexes, cyclotrons in particular [2]. Often, ECRIS output defines the overall performance of the accelerators, especially for very highly charged ions. Since their invention in the mid-sixties, ECRIS performance has shown a remarkable improvement. This progress is mainly due to increasing the frequency of microwave radiation used for plasma heating, accompanied by an appropriate scaling of the magnetic fields. Semi-empirical scaling laws define the directions for source development [2]. Additional tricks, such as gas-mixing, biased-disk, frequency tuning and others, boost the extracted currents. Each new ECRIS generation brings larger and more expensive sources, particularly since the introduction of fully super-conducting sources, with smaller margins for errors in source design.

Computer simulation of physical processes in ECRIS may pave the way for further improvement of the sources. In order to do so, a computer code should be able to reproduce the main features of ECRIS behaviour. However, this is far from trivial due to difficulties in describing the complex non-linear processes in the source plasma. Calculations are limited by the lack of an adequate understanding of the involved phenomena and by the available computational capabilities. A partial solution could be the use of so-called "toy-models", where some plasma parameters are adjustable or are considered as input, and the relative importance of various effects can be studied.

In this paper we present some new developments of such "toy-model" used in our PIC-MCC code for the simulation of ECRIS behaviour [1]. In the first version of the code, we described the ECRIS performance by assuming that the ECR plasma is free to flow along the magnetic field lines, with no additional mechanisms for plasma confinement. The experimentally observed charge-state-distributions of the extracted ion currents could be reproduced, as well as the spatial distributions of the extracted ion beams. The ion density gradients play a crucial role, being defined in the calculations by the length of the plasma. Despite the success in modelling, at least one important feature of ECRIS operation was missed – saturation and decrease in the currents of the highest charge states with increasing gas flow into the source chamber. Reaction of the extracted currents to changes in injected RF power was also not correctly described by the model.

As a next step in the development, we suppose that the ECRIS plasma is mainly localized inside ECR zone and that the ions are transported toward the source wall beyond this zone by a (pre)sheath electric field. However, an additional confining mechanism is now needed to reproduce the experimental CSD of the ion currents, and we assume that it is due to a ponderomotive barrier close to the ECR boundary [3]. Indeed, there is experimental evidence of a modification of the plasma profile caused by intense microwave radiation. A ponderomotive force pushes electrons from regions where the radiation power density is highest, and the emerging potential barrier confines ions. Such regions occur for example when the plasma density is close to the critical or quarter-of-critical value [4], or the magnetic field is close to the ECR condition.

There are models [5] that describe absorption of the microwave radiation at the ECR surface and electron heating in terms of non-linear decay of microwaves into electrostatic electron waves that propagate along the magnetic field lines toward the upper-hybrid-resonance (UHR) layer, where they are absorbed. We remind that the UHR layer is situated where $\omega^2_{RF}=\omega^2_p+\omega^2_c$, with ω_{RF} the microwave frequency, ω_c the cyclotron frequency, and ω_p the plasma frequency. In this approach, the highest gradients of the wave electric field are at the UHR layer.

We present the results of calculations based on the assumption that the ECRIS plasma is located mainly inside the UHR layer and is confined by a potential barrier. Despite the unavoidable simplifications and assumptions, we are able to reproduce the charge-state

ISBN 978-3-95450-128-1

and spatial distributions of the extracted ion beams for our A-ECR ion source, as well as the main features of the source response to changes in the operational parameters. Some specific aspects of the source operation have been examined in detail and will be discussed below.

CODE DESCRIPTION

The main algorithm of the code follows the standard particle-in-cell technique using the Boris mover for tracking the motion of ions in magnetic and electric fields. The magnetic field is calculated for the parameters of the KVI A-ECR ion source [6], with a hexapole magnetic field of 0.75 T at the plasma chamber walls, an injection field of 2 T and an extraction field of 1 T. The electric field is set to zero inside the UHR zone while in the outer region it is along the magnetic field lines. Simulations show that the electric field strength in this region can be varied in a wide range without changing the results providing that there is no back-reaction of the accelerated ions on the processes inside the dense parts of the plasma.

In addition to the Larmor motion of the ions in the magnetic field and their acceleration along the magnetic field lines, ions are elastically colliding with each other. These collisions are treated using the standard Takizuka-Abe method [7] that conserves both energy and momentum of the colliding partners. The electron density is calculated from the condition of charge-neutrality; the electron temperature is a free parameter chosen to obtain the best correspondence between the simulations and experiments. In all our simulations the electron temperature has been set to 1 keV close to the value estimated from dedicated simulations of X-ray emission from ECRIS plasmas [8].

When ions hit the walls, they are assumed to be accelerated to energies that correspond to the plasma potential (25*Q eV is a typical value, with Q the ion charge) and reflected as atoms while losing 80% of their energy [9]. The neutral particle motion is followed taking into account the energy losses during the atom collisions with the walls. Thermal accommodation coefficients are taken from [10]. These coefficients define the ratio between the initial energy of an atom impinging on the wall and its energy after reflection. The coefficients depend on the atomic mass and wall material. For noble gases such as neon and argon, the coefficients are around 0.6 for energies above of a few eV and go to small values (less than 0.1) for energies in the meV range.

Charge-changing and elastic scattering collisions between ions and atoms are treated using rates from Phelps [11]. When the initial charge of the colliding ion exceeds 1+, the Coloumb repulsion of the charge-changed pair of ions results in a kinetic energy release that is estimated to be around 10 eV. It should be noted, however, that charge-changing collisions do not play an important role in the plasma dynamics both due to the relatively small collision rates and low density of the neutral particles inside the dense parts of the plasma. Charge-changing collisions between ions can be neglected because of their low rates.

To calculate the extension of the UHR zone, it is necessary to calculate the average value of the electron density inside the dense parts of the plasma; otherwise the numerical noise in the calculations results in unreliable data. The averaging is justified by the fact that the plasma density inside the confined area is almost uniform, both along the magnetic field lines and across the field in the central parts around the source axis. In the minimum-B configuration of the ECRIS magnetic field, the UHR boundary is a closed surface located inside the ECR layer (defined by the condition of |B|=0.5 T for RF frequency of 14 GHz) and coincides with the ECR layer in the limit of zero plasma density. With increasing plasma density, the size of the UHR zone decreases.

In the simulations, when ions cross the UHR zone boundary, they are either reflected back, depending on their energy and charge state, or accelerated toward the walls and extraction aperture in the electric field of the presheath. The potential barrier at the UHR boundary is on top of the positive plasma potential in respect to the chamber walls. The barrier varies spatially and depends on a number of plasma parameters, e.g. the RF mode structure of the plasma chamber, the injected RF power etc. It is very difficult to calculate its value. For the moment we have side-stepped this problem by assuming the barrier height to be a global constant. It is a free parameter in our simulations varying in the range from zero to a few Volts.

RESULTS

The spatial distribution of ions hitting the extraction electrode of the source is shown in Fig. 1.

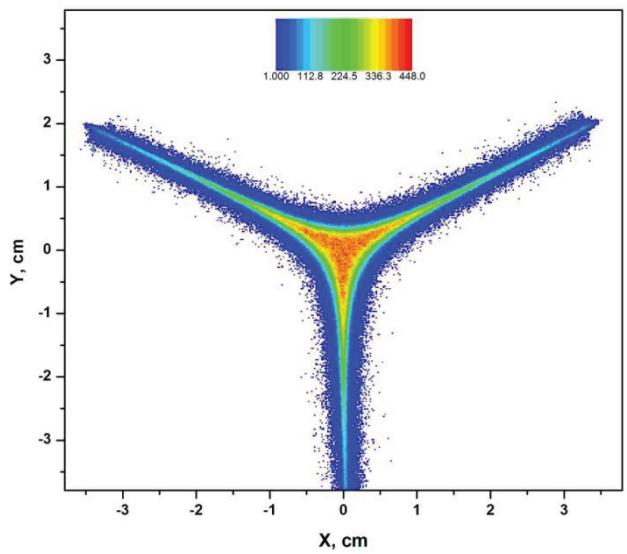

Figure 1: Spatial distribution of ion flux onto the extraction electrode.

The characteristic three-arm star structure is visible with sharp narrow stripes in the middle of diffuse arms. The pattern reproduces the experimentally observed

ISBN 978-3-95450-128-1

sputter marks well. The highly charged ions are localized close to the source axis, whereas the halo is mainly due to the lowly charged ions.

The ratio between the ion flux into the 8-mm diameter extraction aperture and the total flux onto the extraction electrode varies from 0.25 for Ar^{1+} to 0.4 for Ar^{11+}. No hollow beams are observed and the extracted beam profile is predicted to have the triangular shape as it is observed experimentally [12]. The profile is less concentrated on the axis as compared to the simulation results of [1] where we did not assume plasma confinement by a potential barrier. Also, the narrow stripes were not visible in the profiles presented in [1].

The gas temperature inside the source chamber is close to room temperature although the heating mechanism due to creation of energetic atoms after reflection of ions from the walls is taken into account. As a result, very few atoms are able to penetrate into the dense parts of the plasma without ionization. A hollow gas density profile is formed as shown in Fig. 2. The argon density is calculated in a slice of 2 cm at the center of the plasma chamber.

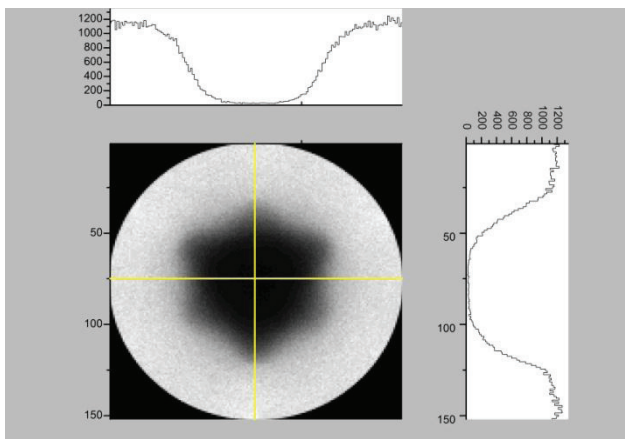

Figure 2: Neutral argon density in the center of the plasma chamber. Profiles of the density are shown along the corresponding lines in the vertical and horizontal directions.

From these profiles, it is seen that the gas pressure drops from the periphery to the plasma center by three orders of magnitude. A strong ion-pumping effect is observed, with the particle flux into the extraction aperture consisting almost completely of ions - the neutral particle flux is less than 15% of the total flux. In steady conditions, the flow of particles out of the system through the extraction is equal to the gas flux into the source chamber. In the following, we use this value to characterize the source performance instead of the gas pressure in the chamber.

Experimentally observed charge-state-distributions of the extracted ion current can be accurately reproduced with our code, as shown in Fig. 3 for argon and neon.The experimental spectra were obtained by tuning the source to maximize the currents of Ar^{8+} and Ne^{6+} respectively. Mode jumps limited the source performance above these conditions. No normalization of the simulation data have been done and we compare the absolute values without accounting for the beam losses in the beam line.

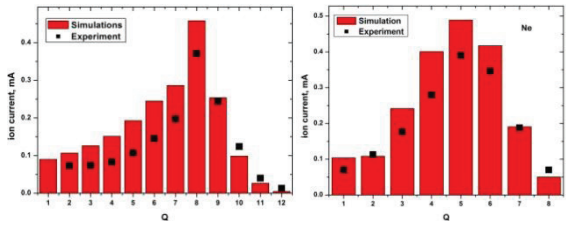

Figure 3: Experimentally measured charge-state-distributions of the extracted currents (squares) and the simulated spectra for argon and neon plasmas.

The variation of the simulated argon ion currents with gas flow into the source is presented in Fig. 4.

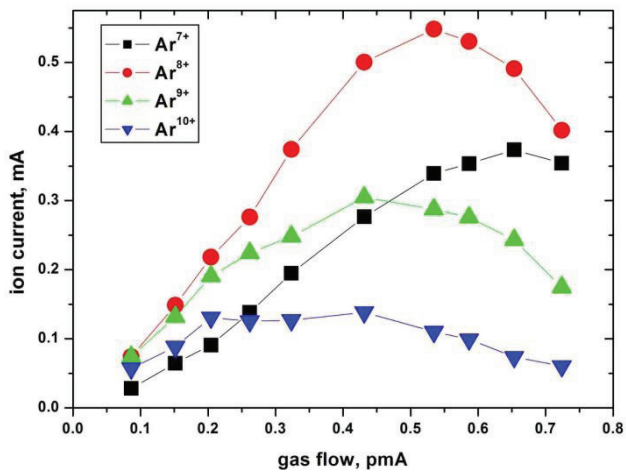

Figure 4: Currents of Ar^{7+}-Ar^{10+} ions as a function of the gas flow into/out of the source.

Currents of relatively high charge state ions (higher than 8+ for argon) saturate with increasing gas flow and then decrease. The lower charge states are still increasing, resulting in "colder" spectra and decrease of the mean charge state of the extracted currents. Such behavior is consistent with experimental observations. The reason for saturation and decrease of the highly charged ion currents (HCI) is decrease of the plasma size due to shrinking of the UHR zone with growing plasma density. For the gas flows in Fig. 4 that correspond to a maximal current of Ar^{8+} ions, the plasma density is close to 7×10^{11} cm^{-3}, well below the critical value of 2.5×10^{12} cm^{-3} for 14 GHz microwaves.

Ion currents as a function of the potential barrier height are shown in Fig. 5 and have been calculated by varying the statistical weight of the super-particles such as to keep the total flux of the particles into the extraction aperture constant. For small barrier values, the ion confinement is weak and almost no highly charged ions are produced.

With increasing barrier height, currents are increasing up to a certain level and then saturate. The saturation is connected to a shrinking of the plasma with increasing plasma density, in the same manner as occurs for high gas

flows into the source (Fig. 4). Such behavior should be compared to the experimental dependencies of the extracted currents with varying the injected RF power as shown in Fig. 6.

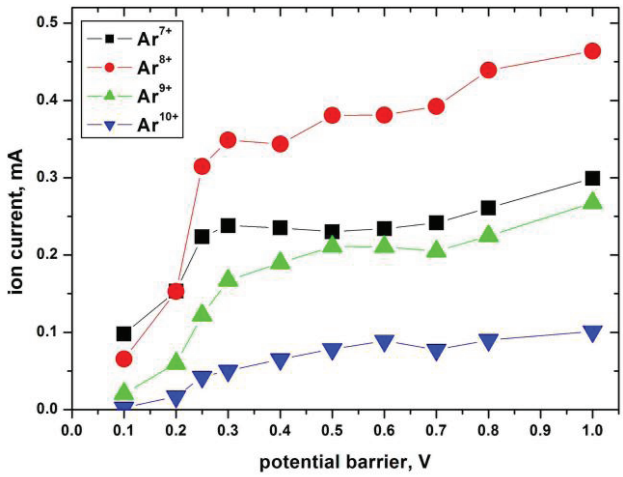

Figure 5: Currents of Ar^{7+}-Ar^{10+} ions as a function of the potential barrier height.

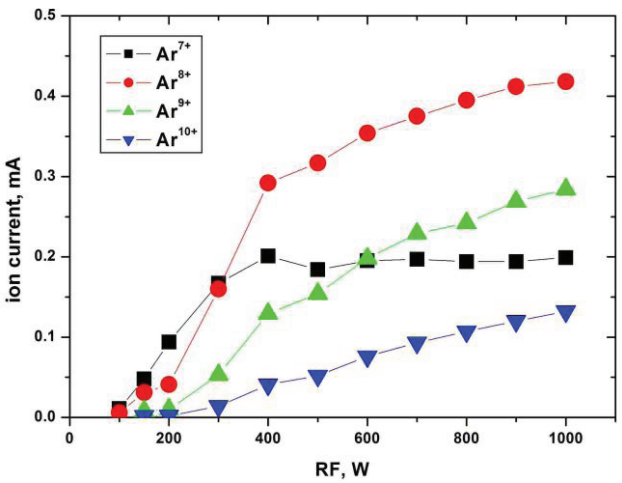

Figure 6: Experimental dependencies of the extracted ion currents on the injected RF power.

The currents have been measured while keeping the gas flow into the chamber at the same level that maximizes the Ar^{8+} current. Currents of the high charge states increase fast above RF powers of 100 W and then tend to saturate. This is consistent with the dependence shown in Fig. 5, since the potential barrier height is determined by the intensity of the microwave radiation inside the source.

It is known that the currents of highly charged ions can be increased by injecting a lighter gas into the source – the so-called gas-mixing effect [13]. The opposite effect occurs, i.e. a degradation of source performance, when heavy impurity ions are present in the ECRIS plasma. To check it, we performed simulations with mixing helium and argon to compare it with pure argon. When the helium flux is optimized, the currents of the highest charge states are increased by factor of 2. A dependence of the Ar^{10+} current on the helium flux is shown in Fig. 7.

Furthermore, the argon ion temperature is substantially lower in a He-Ar mixture. If collisions between helium and argon are switched off in the calculations, then the currents of the argon HCI decrease, but they are still higher than in the case of a pure argon plasma. With no He-Ar collisions, the He^{2+} current increases by a factor of three. From this, we conclude that the gas-mixing effect is partially due to the evaporative cooling of ions. Modification of the plasma radial profile is also observed to play an important role since helium atoms more easily penetrate the dense parts of the plasma with their higher ionization potential and higher velocities compared to argon.

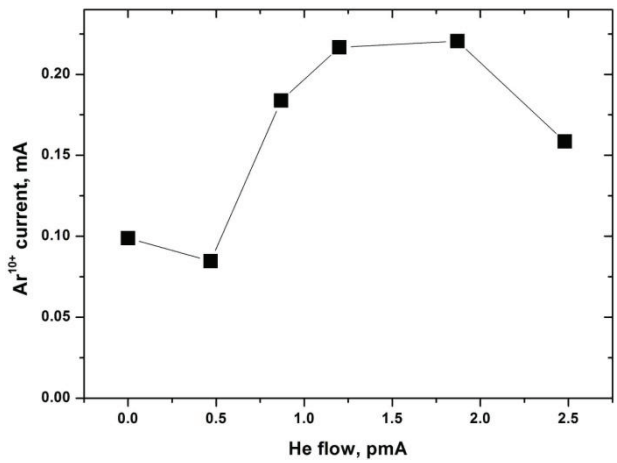

Figure 7: Calculated current of Ar^{10+} ions for different helium fluxes into the source.

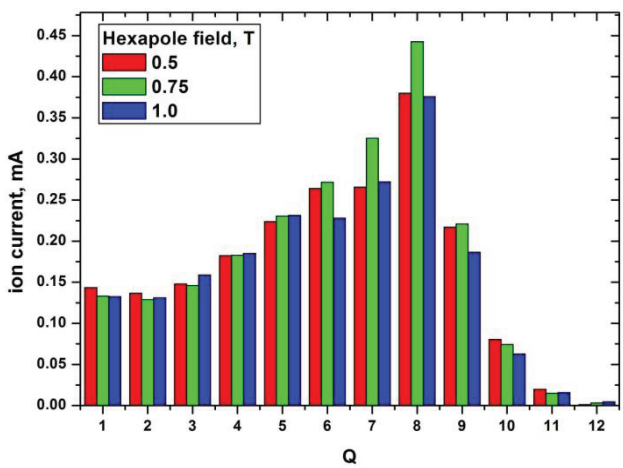

Figure 8: Charge-state distributions of the argon ions for the different hexapole magnetic fields at the radial wall.

We have also performed calculations with varying magnetic field parameters. Charge-state distributions of argon ions are shown in Fig. 8 for different hexapole magnetic field value at the source radial wall. The calculation were done with changing the statistical weight of the super-particles to keep the output flux at the same level.

A large hexapole field results in a decrease of the HCI currents because the plasma becomes smaller in the radial direction. When the field is lower than the optimal value,

ISBN 978-3-95450-128-1

the plasma size increases, but the currents decrease due to the broader plasma profiles at the extraction electrode and more efficient screening of the dense parts of the plasma from the atom fluxes.

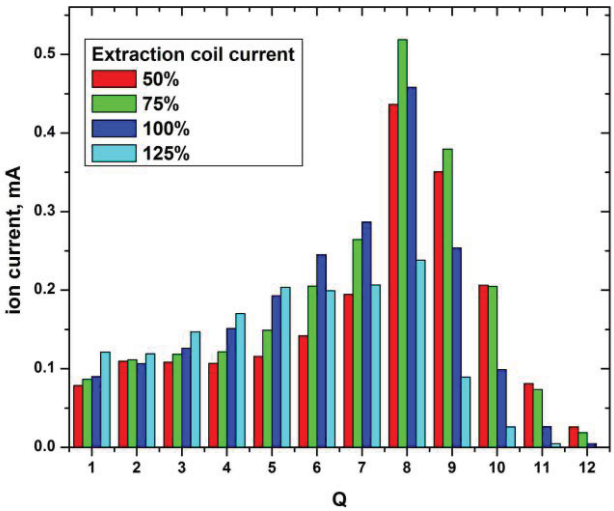

Figure 9: Extracted ion currents for the different currents in the extraction solenoid.

The spectra of extracted ion currents have also been calculated for different currents in the solenoid coil at the extraction side of the source. These distributions are shown in Fig. 9.

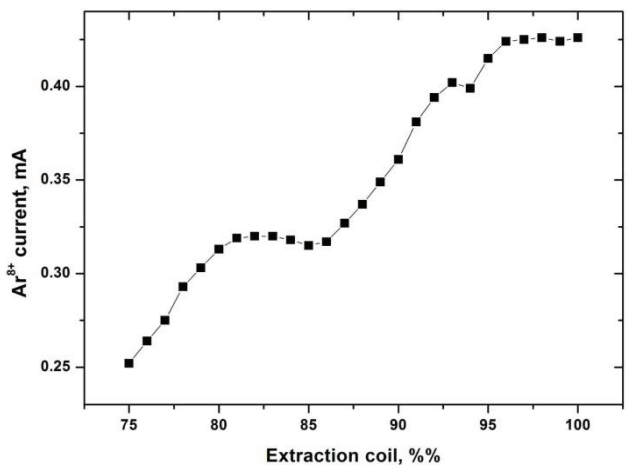

Figure 10: The experimental dependence of Ar^{8+} current on the current in the extraction coil.

HCI currents are maximized when the extraction magnetic field is lower than the nominal value that corresponds to full energization of the extraction solenoid. This is in strong contradiction with the experimentally observed behavior. In our source, the maximal currents of argon ions are obtained when maximizing the current in the extraction coil. The experimental dependence of the Ar^{8+} current on the current in the extraction coil is shown in Fig. 10.

In the simulations a lower magnetic field at the extraction side of the source leads to a larger size of the confined plasma since the ECR and UHR zones increase. In the experiment, the ion current is almost doubled when the coil current is varied from 75% to 100%. It is seen, however, that the experimentally measured current does not monotonically increase with the magnetic field. This probably indicates some variations in the RF intensity pattern in the source chamber cavity and onset of plasma instabilities.

CONCLUSIONS

The computational model described in this paper reproduces the main features of ECRIS performance. It is based on the assumption that ECR plasma is confined inside the upper-hybrid resonance zone by a potential barrier produced by the ponderomotive force. The simulated extracted ion currents are close to the experimental values. Responses of the source performance to variations in the gas flow and RF injected power are reproduced. The gas-mixing effect is also observed and found to be mainly due to the evaporative cooling of ions. Profiles of the extracted ion currents are obtained that can be used in particle transport simulations.

ACKNOWLEDGMENTS

This work is part of the research program of the "Stichting voor Fundamenteel Onderzoek der Materie" (FOM) with financial support from the "Nederlandse organisatie voor Wetenschappelijk Onderzoek" (NWO). It is supported by the University of Groningen and by the "Gesellschaft für Schwerionenforschung GmbH" (GSI), Darmstadt, Germany.

REFERENCES

[1] V. Mironov and J.P.M. Beijers, Phys. Rev. ST Accel. Beams **12**, 073501 (2009).
[2] R. Geller, Electron Cyclotron Resonance Ion Sources and ECR Plasma (Bristol: Institute of Physics), 1996.
[3] A. Ivanov and K. Wiesemann, IEEE Trans. Plasma Sci., **33**, 1743, (2005).
[4] K. Mizuno, J. S. DeGroot, and K. G. Estabrook, Phys. Rev. Lett., **52**, 271 (1984).
[5] G. Castro et al., Rev. Sci. Instrum. **83**, 02B501 (2012).
[6] H.R. Kremers, J.P.M. Beijers, and S. Brandenburg, Rev. Sci. Instrum. 77, 03A311 (2006).
[7] T. Takizuka and H. Abe, J. Comp. Phys. **25**, 205 (1977).
[8] M.C. Martins et al., arXiv:0909.2393 [physics.atom-ph].
[9] X.-Y. Liu et al., Thin Solid Films **422**, 141 (2002).
[10] F.O. Goodman and H.Y. Wachman, J. Chem. Phys. **46**, 2376 (1967).
[11] A. V. Phelps, J. Appl. Phys. **76**, 747 (1994).
[12] S. Saminathan, V. Mironov, J.P.M. Beijers, R. Kremers, and S. Brandenburg, Rev. Sci. Instrum. 81, 02B706 (2010).
[13] G. Melin, A. G. Drentje, A. Girard, and D. Hitz, J. Appl. Phys. 86, 4772 (1999).